



Significantly improved dehydrogenation of ball-milled MgH₂ doped with CoFe₂O₄ nanoparticles



Jiawei Shan^a, Ping Li^{a,*}, Qi Wan^a, Fuqiang Zhai^b, Jun Zhang^a, Ziliang Li^a, Zhaojiang Liu^a, Alex A. Volinsky^c, Xuanhui Qu^a

^a State Key Laboratory for Advanced Metals and Materials, Institute for Advanced Materials and Technology, USTB, Beijing 100083, China

^b Departament Física Aplicada, EETAC, Universitat Politècnica de Catalunya – BarcelonaTech, 08860 Castelldefels, Spain

^c Department of Mechanical Engineering, University of South Florida, Tampa, FL 33620, USA

HIGHLIGHTS

- CoFe₂O₄ has strong catalytic effect on MgH₂ hydrogen storage based on its strong oxidative activity.
- The final reaction products of MgH₂ and CoFe₂O₄ are the ternary combinations: Co₃Fe₇, MgO and Co.
- Co₃Fe₇, MgO and Co combination has a great catalytic effect on MgH₂ hydrogen storage performance.
- MgH₂ hydriding–dehydriding process depends on the methods of adding Co₃Fe₇, MgO and Co.

ARTICLE INFO

Article history:

Received 29 April 2014

Received in revised form

21 June 2014

Accepted 21 June 2014

Available online 7 July 2014

Keywords:

Cobalt ferrite

Hydrogen storage

Magnesium hydride

Dehydrogenation temperature

ABSTRACT

CoFe₂O₄ nanoparticles are added to magnesium hydride (MgH₂) by high-energy ball milling in order to improve its hydriding properties. The hydrogen storage properties and catalytic mechanism are investigated by pressure–composition–temperature (PCT), differential thermal analysis (DTA), X-ray diffraction (XRD), field-emission scanning electron microscopy (FESEM) and transmission electron microscopy (TEM). The nonisothermal desorption results show that the onset desorption temperature of the MgH₂ + 7 mol% CoFe₂O₄ is 160 °C, which is 200 °C lower than of the as-received MgH₂. The dehydrogenation process of the MgH₂ doped with the CoFe₂O₄ nanoparticles includes two steps. DTA curves and XRD patterns reveal that a chemical reaction happens between MgH₂ and CoFe₂O₄, forming the final products of the ternary combination, corresponding to Co₃Fe₇, MgO and Co. The onset desorption temperature of the ball-milled MgH₂ doped with Co₃Fe₇, MgO and Co is about 260 °C, approximately 100 °C lower than the un-doped MgH₂, demonstrating that the ternary combination (Co₃Fe₇, MgO, and Co) also has a great catalytic effect on the MgH₂ hydrogen storage properties. It is also confirmed that the various methods of adding the ternary combination have different effects on the MgH₂ hydriding–dehydriding process.

© 2014 Elsevier B.V. All rights reserved.

1. Introduction

Magnesium hydride has a great potential as one of the promising hydrogen storage candidates for mobile applications due to its high theoretical hydrogen storage capacity of 7.6 wt% [1–4]. Besides, the Mg-based hydrides are abundant and inexpensive [5]. However, the high desorption temperature (>400 °C) and poor dehydriding kinetics prevent MgH₂ practical applications. During the past few decades, extensive efforts have been devoted to

decrease the onset desorption temperature and improve the MgH₂ dehydrogenation kinetics. Among these efforts, catalyst doping by ball milling has attracted considerable attention to improve the MgH₂ hydrogen storage properties. To date, the reported catalysts include transition metals [4,6–11], transition metal oxides [12–18], transition metal halides [19–21] and intermetallic compounds [22,23]. Since the transition metals have multiple valence states, the corresponding transition metal oxides have better catalytic performance with MgH₂ [24], such as Cr₂O₃ and Fe₂O₃ [7,16]. Li et al. [25] also observed the superior effect of Co₂O₃ nanoparticles on promoting the dehydrogenation properties of LiAlH₄ and Co₂O₃ transformed into the new CoO phase. Recently the ternary oxide has been a hotspot of research because of the role it has played in

* Corresponding author. Tel.: +86 10 8237286; fax: +86 10 62334311.

E-mail address: ustbliping@126.com (P. Li).

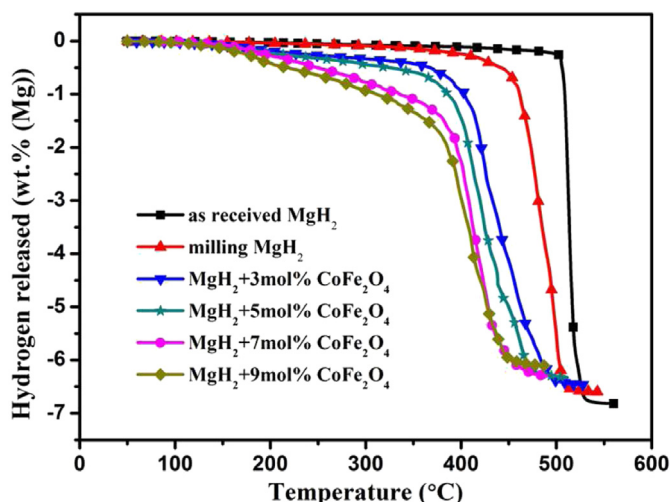


Fig. 1. Thermal desorption curves of the as-received MgH₂, as-milled MgH₂ and ball-milled MgH₂ doped with 3 mol%, 5 mol%, 7 mol% and 9 mol% nanosized CoFe₂O₄.

improving the dehydrogenation properties of hydrogen storage materials. Mandzhukova [26] reported that the presence of NiCo₂O₄ in magnesium composites could improve considerably the hydriding kinetics of magnesium. Meanwhile, the dehydrogenation performance LiAlH₄ catalyzed by NiFe₂O₄ [27] and CoFe₂O₄ [28] nanoparticles have been substantially advanced. It was also

reported that MnFe₂O₄ could significantly improve MgH₂ hydrogen storage performance, and valence-changed iron ions (Fe_{0.872}O) play a key role in remarkably advancing MgH₂ dehydriding properties [29]. Therefore, it is reasonable to believe that CoFe₂O₄ could show great catalytic effect and advance MgH₂ hydrogen storage performance.

In this work, CoFe₂O₄ nanoparticles were utilized as catalyst to investigate their effects on the hydrogen storage properties of MgH₂ prepared by the high-energy ball milling, and the catalytic mechanisms were also analyzed.

2. Experimental details

MgH₂ (99.5% pure, 50 nm) and CoFe₂O₄ ($\geq 99\%$ pure, 40 nm) were obtained from Sigma Aldrich Co., and both materials were used as-received without any purification. All operations were performed in the glove box filled with a high purity argon atmosphere in order to avoid oxidation and humidity. The MgH₂ powder was ball-milled with different proportions (3 mol%, 5 mol%, 7 mol%, 9 mol% and 20 mol% of the total substance amount) of the CoFe₂O₄ nanoparticles. Then the mixture was loaded into a stainless steel milling vial with a ball to powder weight ratio of 20:1. Subsequently, the samples were ball-milled for 30 min by using a high-energy Spex mill (QM-3B) at the rate of 1200 rpm. After each 10 min of the ball milling, the steel vial was rested for 5 min to cool it. The final product of the reaction between MgH₂ and 20 mol% CoFe₂O₄ nanoparticles is directly mixed with MgH₂ by the ball milling, and the amount is the same as from the reaction between MgH₂ and 7 mol% CoFe₂O₄ nanoparticles.

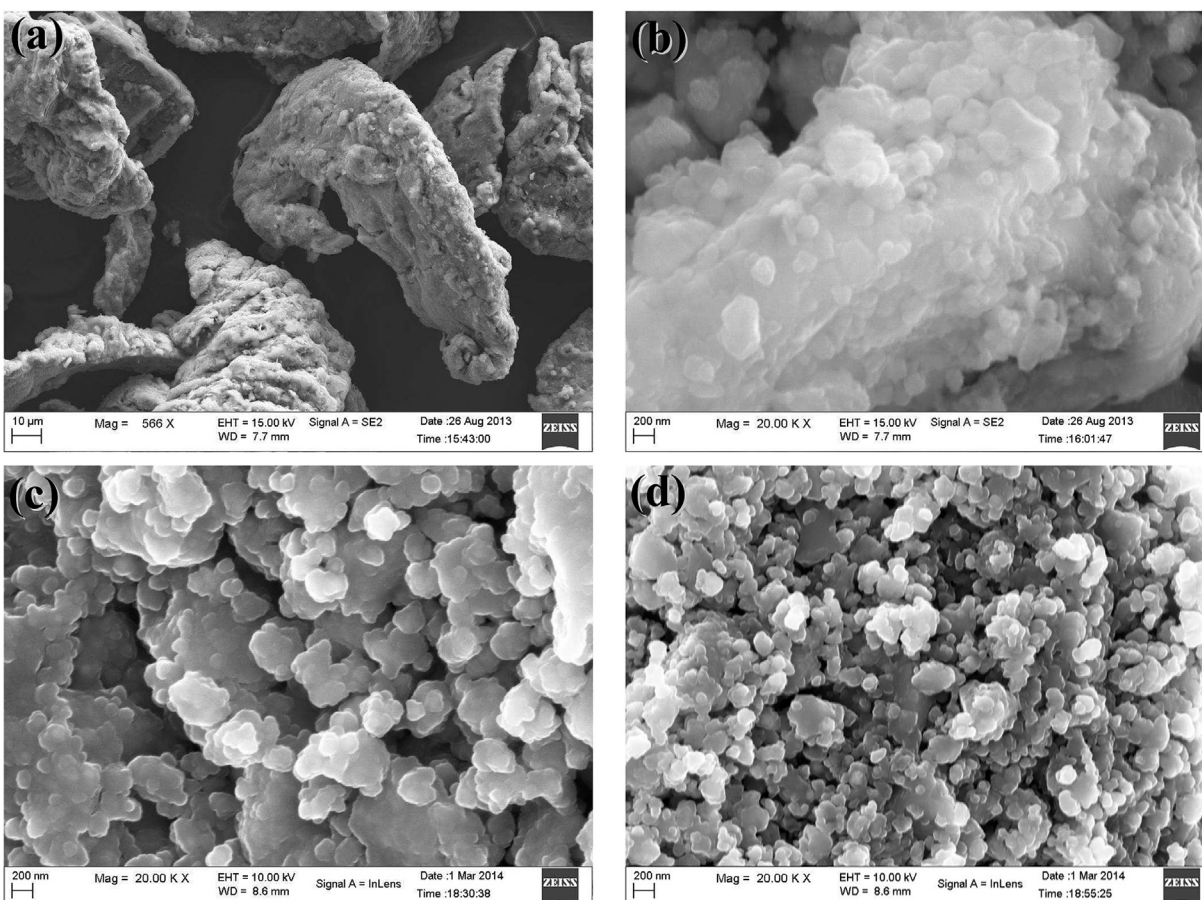


Fig. 2. SEM images of: (a) the as-received MgH₂, (b) as-milled MgH₂, ball-milled MgH₂ doped with (c) 3 mol%, and (d) 7 mol% nanosized CoFe₂O₄.

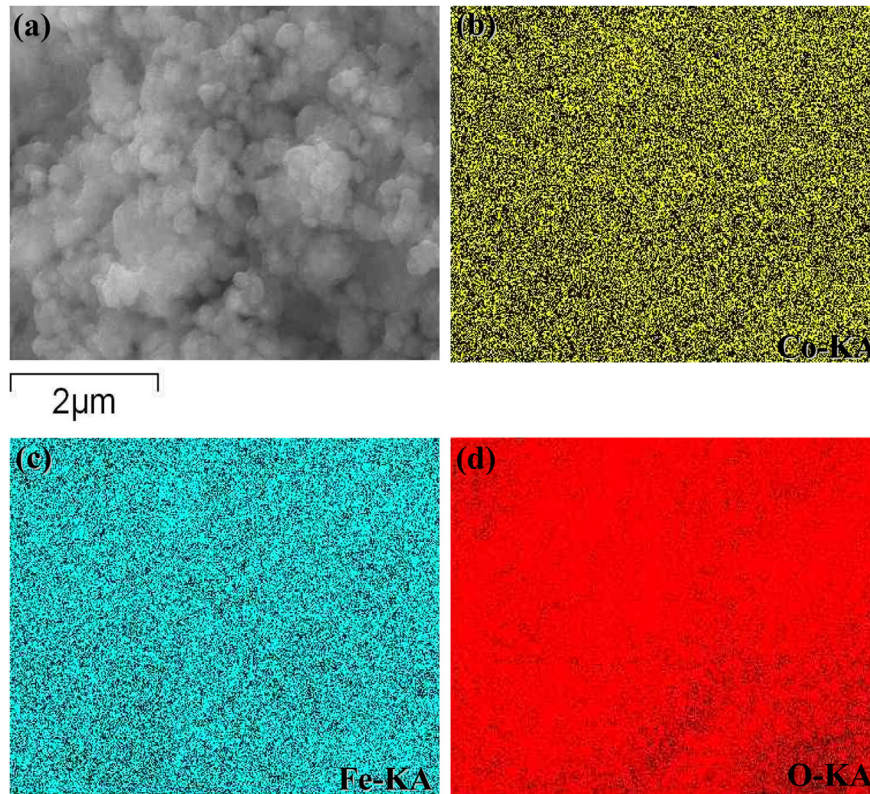


Fig. 3. (a) FESEM image of ball-milled MgH_2 with 7 mol% CoFe_2O_4 and elemental maps of: (b) Co, (c) Fe and (d) O.

The dehydrogenation properties of the as-received MgH_2 and doped samples were measured using a pressure-composition-temperature (PCT) apparatus (Beijing Nonferrous Metal Research Institute, China). This apparatus can be operated up to 10 MPa and 600 °C. It mainly consists of a pressure transducer and a reactor. The reactor has two parts, the heater and the sample vessel. From the magnitude of the hydrogen pressure change, one can calculate the amount of the absorbed and desorbed hydrogen. Typically, 0.3 g sample was loaded into the vessel, and then heated up to 500 °C at a 6 °C min^{-1} rate under vacuum. Following the first complete dehydrogenation, the samples were subjected to rehydrogenation under 6 MPa hydrogen pressure at 350 °C. In order to further analyze the dehydrogenation performance of the MgH_2 samples

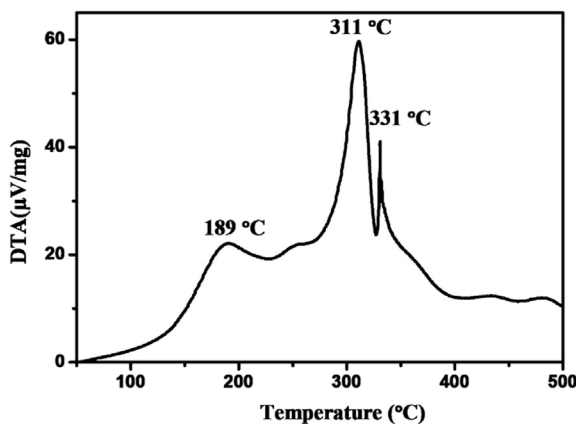


Fig. 4. DTA curves of ball-milled MgH_2 doped with 7 mol% CoFe_2O_4 within the 50–500 °C temperature range at a heating rate of 5 °C min^{-1} .

doped with CoFe_2O_4 nanoparticles, the differential thermal analysis (DTA) with WSC-DTA was conducted to investigate the thermal behavior of the samples with an argon flow rate of 50 ml min^{-1} and a heating rate of 10 °C min^{-1} , from 50 °C to 500 °C.

The morphology and microstructure of the un-doped and doped samples after ball milling and after dehydrogenation were examined by the field-emission scanning electron microscopy (FESEM, ZEISS ULTRA55, Germany) and transmission electron microscopy (TEM). The samples were ultrasonically dispersed in the alcohol

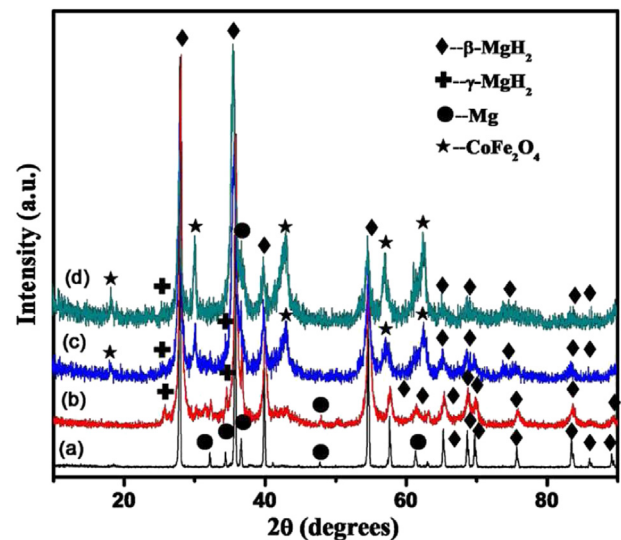


Fig. 5. XRD patterns of: (a) as-received MgH_2 , (b) as-milled MgH_2 , (c) ball-milled MgH_2 doped with 3 mol% CoFe_2O_4 and (d) ball-milled MgH_2 doped with 7 mol% CoFe_2O_4 samples.

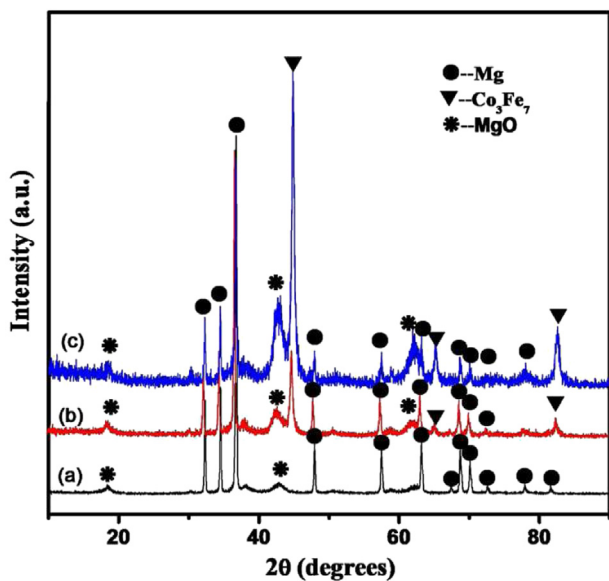


Fig. 6. XRD patterns of: (a) as-milled MgH₂, (b) ball-milled MgH₂ doped with 3 mol% CoFe₂O₄ and (c) ball-milled MgH₂ doped with 7 mol% CoFe₂O₄ after dehydrogenation.

solution. A drop of the suspension was placed on a 3 mm Cu grid before being loaded into the chamber of the Tecnai G2 F30 S-TWIN TEM. The microscope was operated in the bright field mode with 300 kV accelerating voltage to obtain the sample microstructure and catalyst distribution around the MgH₂ matrix. During the TEM observations, the elemental composition of the tested sample was obtained by the energy dispersive X-ray spectroscopy (EDX). The phase structure of the as-prepared sample was determined by using the MXP21VAHF X-ray diffractometer (XRD with CuK α radiation, 40 kV, 200 mA) at room temperature. The 2 θ angle was varied from 10° to 90° with a scan rate of 0.02° per second.

3. Results and discussion

3.1. Dehydrogenation temperature

The initial desorption temperature is determined by tangent method, and the temperature at where the differential coefficient

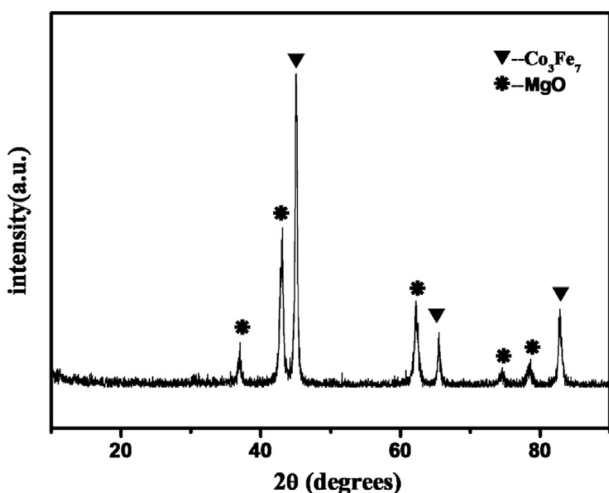


Fig. 7. XRD patterns of ball-milled MgH₂ doped with 20 mol% CoFe₂O₄ after dehydrogenation.

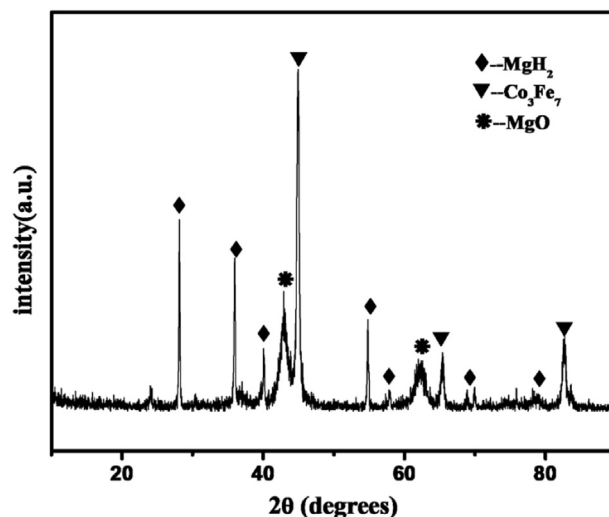


Fig. 8. XRD patterns of the ball-milled MgH₂ doped with 7 mol% CoFe₂O₄ after rehydrogenation.

suddenly changes could be considered as the onset temperature for H₂ desorption. Fig. 1 shows the non-isothermal desorption curves of the as-received MgH₂, as-milled MgH₂, and MgH₂ doped with 3 mol%, 5 mol%, 7 mol% and 9 mol% CoFe₂O₄ nanopowders. It is obvious that adding CoFe₂O₄ nanoparticles dramatically improves the MgH₂ dehydrogenating properties. The as-received MgH₂ starts to release hydrogen at around 440 °C and desorbs about 7 wt% hydrogen, and the initial dehydrogenation temperature of the as-milled MgH₂ is 360 °C, which is by 80 °C lower, compared with the as-received MgH₂.

CoFe₂O₄ nanoparticles significantly reduce the MgH₂ desorption temperature, compared with the un-doped sample. The dehydrogenation process of MgH₂ doped with 3 mol% CoFe₂O₄ initiates at about 200 °C. For the 5 mol% CoFe₂O₄ doped sample, the dehydrogenation process proceeds at 180 °C. Further increase of the additive amount to 7 mol%, causes the doped sample to desorb at 160 °C. With the CoFe₂O₄ amount increasing to 9 mol%, the onset dehydrogenating temperature declines to 150 °C, which demonstrates the CoFe₂O₄ contribution for improving the MgH₂ dehydrogenation

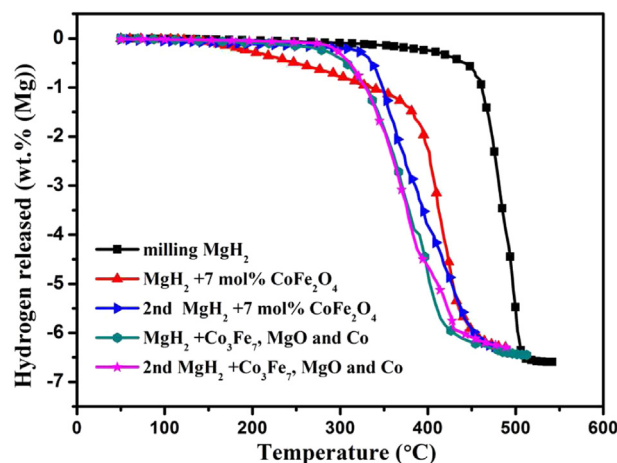


Fig. 9. Dehydrogenation and the second dehydrogenation curves of the ball-milled MgH₂ doped with 7 mol% nanosized CoFe₂O₄ and the same amount of the ternary combination (Co₃Fe₇, MgO and Co) as from the reaction between MgH₂ and 7 mol% CoFe₂O₄ nanoparticles.

onset temperature. Compared with the as-milled MgH_2 , the 3 mol%, 5 mol%, 7 mol% and 9 mol% doped samples cause about 160 °C, 180 °C, 200 °C and 210 °C reduction in the onset dehydrogenation temperature, respectively. During the desorption process, the 3 mol% CoFe_2O_4 doped sample desorbs 6.59 wt% hydrogen, while 6.46 wt%, 6.32 wt% and 6.11 wt% hydrogen are released from the 5 mol%, 7 mol% and 9 mol% CoFe_2O_4 doped samples, respectively.

The 9 mol% CoFe_2O_4 doped sample has the lowest onset dehydrogenation temperature. However, the desorption capacity of the 9 mol% doped sample also decreases, and the effect on hydrogen storage performance of the MgH_2 is very similar to that of the 7 mol% doped sample. Thus, the amount of additive should be as little as possible. Therefore, through comprehensively considering the above analyses, the $\text{MgH}_2 + 7 \text{ mol\% CoFe}_2\text{O}_4$ sample exhibited optimal dehydrogenation performances, including the onset dehydrogenation temperature and the released hydrogen capacity. Thus, 7 mol% CoFe_2O_4 nanoparticles were used to analyze the catalytic effect and the mechanism of CoFe_2O_4 in the following tests.

3.2. Dehydrogenation mechanism

Fig. 2 shows the microstructures of the as-received MgH_2 , as-milled MgH_2 , ball-milled MgH_2 doped with 3 mol%, and 7 mol% nanosized CoFe_2O_4 observed by the scanning electron microscopy (SEM). The mean particle size of as-received MgH_2 is between

30 μm and 50 μm . However, the particle size of the as-milled MgH_2 is between 1 μm and 4 μm and many small particles agglomerate to some extent, as seen in Fig. 2(b), which harms the kinetics of the MgH_2 matrix [30].

After doping with 3 mol% CoFe_2O_4 nanoparticles, the original particle size of MgH_2 is significantly reduced, ranging from 400 nm to 1 μm , as seen in Fig. 2(c). At the same time, the doped samples don't exhibit small particle agglomeration anymore. This is one of the reasons for adding CoFe_2O_4 nanoparticles, which dramatically improves the MgH_2 kinetics. By further increasing the additive amount to 7 mol%, the particle size is reduced more remarkably, ranging from 200 nm to 400 nm. To get the distribution of the elements in the CoFe_2O_4 doped- MgH_2 sample, the EDS mapping of the ball-milled MgH_2 doped with 7 mol% CoFe_2O_4 is carried out, shown in Fig. 3. The distribution of all constitutive elements after ball milling is homogeneous. This means that the catalysts are well mixed with MgH_2 after ball milling, resulting in a high surface defect density and more grain boundaries.

As seen in Fig. 1, the doped samples exhibit similar decomposition processes, which include two dehydrogenation steps. To further investigate this phenomenon and reaction mechanism between CoFe_2O_4 and MgH_2 , the differential thermal analysis (DTA) was performed. Fig. 4 shows the DTA curves of the as-milled MgH_2 doped with 7 mol% CoFe_2O_4 within the 50–500 °C temperature range at a heating rate of 5 °C min^{-1} . As seen in Fig. 4, it is obvious that there are three distinctive peaks. The last two

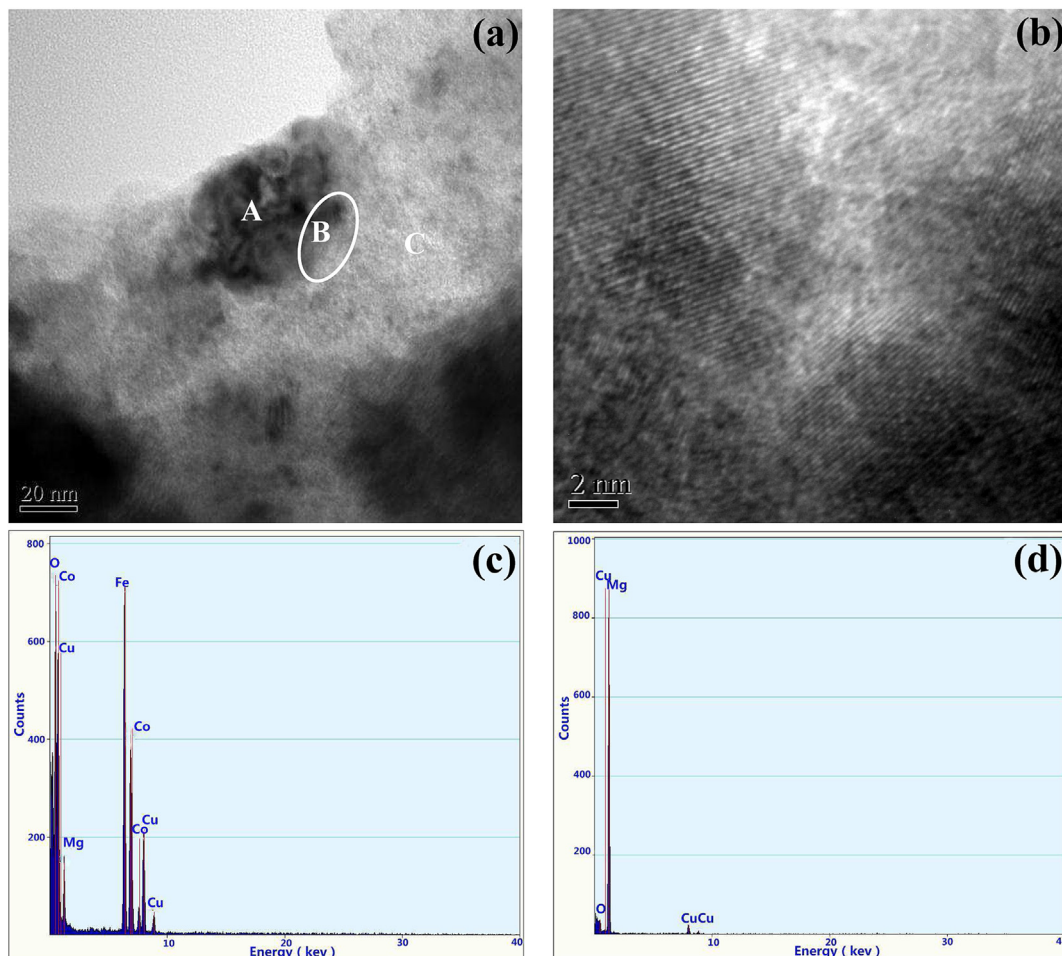


Fig. 10. (a) TEM morphology and (b) HRTEM boundaries micrographs of black and bright regions, EDX: (c) black region, (d) bright region results of MgH_2 with 7 mol% CoFe_2O_4 after ball milling.

endothermic peaks appear at about 311 °C and 331 °C, correspond to MgH₂ (γ -MgH₂, β -MgH₂) desorption [31,32], respectively. The 311 °C peak is attributed to the decomposition of γ -MgH₂, which is mainly transformed from β -MgH₂ during the ball milling processing, and the higher temperature peak is attributed to the desorption from the remnant β -MgH₂. However, the first endothermic peak at 189 °C may be related to the reaction between CoFe₂O₄ and MgH₂.

In order to confirm the reaction of the first endothermic peak, the phase compositions of the as-prepared samples are determined by XRD. Fig. 5 presents XRD patterns of the as-received MgH₂, as-milled MgH₂, ball-milled MgH₂ doped with 3 mol% CoFe₂O₄ and ball-milled MgH₂ doped with 7 mol% CoFe₂O₄ samples. For the as-received MgH₂ sample, almost all diffraction peaks correspond to the β -MgH₂ phase, except a few reflections corresponding to Mg. However, for the as-milled MgH₂ sample, the XRD pattern has broad diffraction peaks, indicating grain refinement due to the high-energy ball milling, which usually occurs when crystals are refined by the mechanical milling processes [16]. The most intense diffraction peak is also identified as β -MgH₂, however, a new γ -MgH₂ phase is also observed [19]. The peak intensities of the CoFe₂O₄ phase increase with increasing of the amount of the CoFe₂O₄ nanoparticles, while the peak intensities of the MgH₂ phase decline, indicating that no reaction between MgH₂ and CoFe₂O₄ occurs during the ball milling process.

XRD patterns of the as-milled MgH₂ as well as the 3 mol% and 7 mol% CoFe₂O₄ doped samples after dehydrogenation are shown in Fig. 6. For the as-milled MgH₂, it can be seen that the sample only has the Mg phase, except for minor MgO reflections, which are probably due to oxygen contamination during the sample preparation after dehydrogenation. For the 3 mol% CoFe₂O₄ doped samples, Mg, Co₃Fe₇ and MgO are found, and diffraction peaks of the MgO and Co₃Fe₇ phases gradually enhance, with increasing the CoFe₂O₄ amount to 7 mol%, indicating that MgH₂ reacts with CoFe₂O₄ during the heating process. A similar decomposition reaction occurs between CoFe₂O₄ and H₂, where CoFe₂O₄ will reduce to Co₃Fe₇ and Co [33]. Thus, it is reasonable to believe that the Co element is also one of the products from the reaction between MgH₂ and CoFe₂O₄. Since Cu radiation is used in the XRD measurements, the XRD measurement is not useful for the Co element in composites because of the Cu K α radiation [34]. The whole dehydrogenation process may be written as:



In order to demonstrate the above process, MgH₂ is mixed with 20 mol% CoFe₂O₄ nanoparticles by ball milling, then heated up to 500 °C to make sure that MgH₂ and CoFe₂O₄ fully react. The final products are shown in Fig. 7. As seen in Fig. 7, Co₃Fe₇ and MgO phases still exist, while Mg disappears. This phenomenon proves

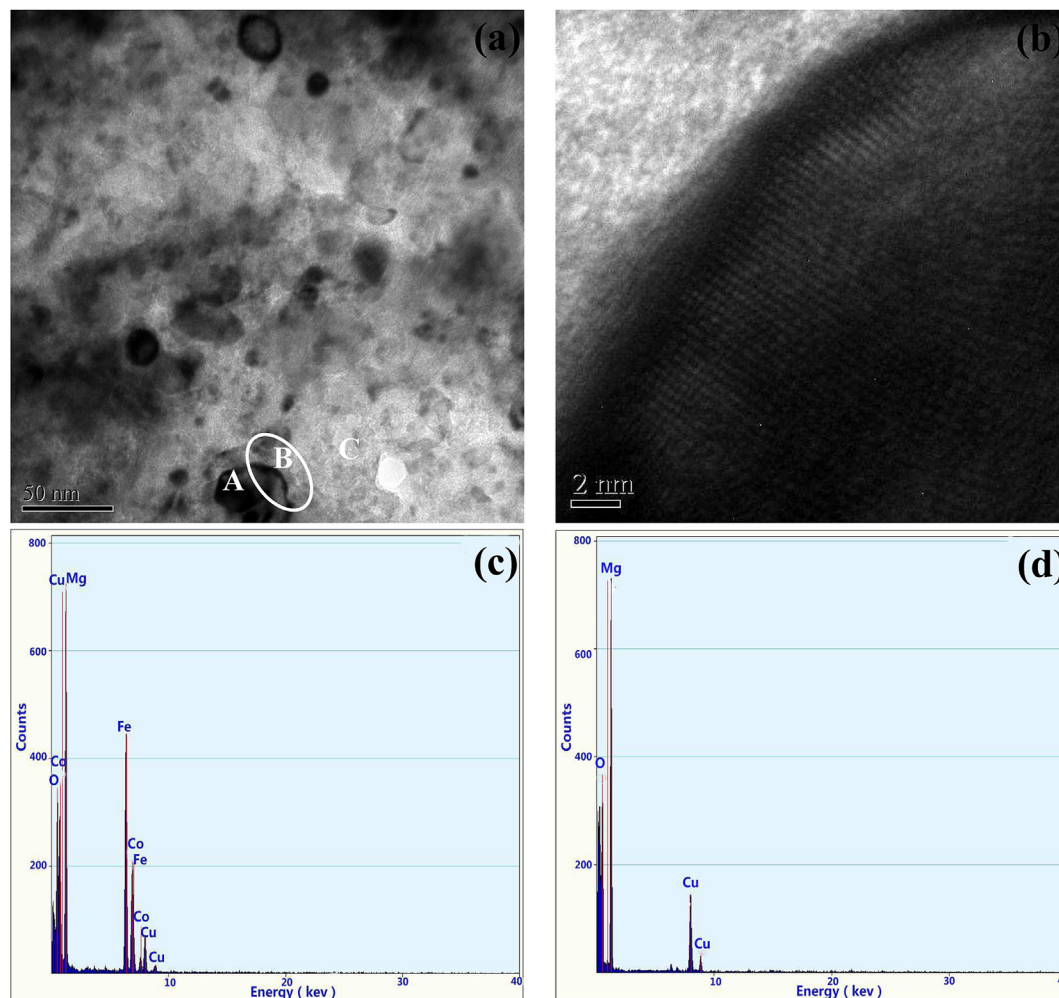


Fig. 11. (a) TEM morphology and (b) HRTEM boundaries micrographs of the black and bright regions, EDX: (c) black region, (d) bright region results of the ball-milled MgH₂ with 7 mol% CoFe₂O₄ after the second dehydrogenation.

that when the ratio of moles in the MgH_2 and CoFe_2O_4 phases is 4:1, the chemical reaction between MgH_2 and CoFe_2O_4 will be carried out adequately. This is sufficient to prove that MgH_2 can react with CoFe_2O_4 at about 189 °C.

Following the first complete dehydrogenation, the samples were subjected to rehydrogenation under 6 MPa hydrogen pressure at 350 °C. Fig. 8 shows the XRD patterns of the ball-milled MgH_2 doped with 7 mol% CoFe_2O_4 after rehydrogenation. Compared with the mixed sample after the dehydrogenation, Co_3Fe_7 and MgO phases do not change, while Mg is transformed into MgH_2 , indicating that the ternary combination (Co_3Fe_7 , MgO and Co) is very stable. Therefore, CoFe_2O_4 nanoparticles play a role just in the first MgH_2 dehydrogenation. In the next hydriding–dehydrating cycles, Co_3Fe_7 , MgO and Co are the main phases that affect hydrogen storage properties of MgH_2 .

For the sake of testing whether ternary combination (Co_3Fe_7 , MgO and Co) plays a catalytic role in hydrogen desorption of MgH_2 , the ternary combination (Co_3Fe_7 , MgO and Co) is added into the MgH_2 matrix by two different methods: (1) 7 mol% CoFe_2O_4 is added into the MgH_2 matrix and reacts with the MgH_2 , and the final reaction products are the catalysts. (2) The ternary combination (Co_3Fe_7 , MgO and Co), which is the final product of the reaction between MgH_2 and 20 mol% CoFe_2O_4 nanoparticles, is directly mixed with the MgH_2 by the ball milling, and the amount is the same as with Co_3Fe_7 , MgO and Co from the reaction between MgH_2 and 7 mol% CoFe_2O_4 nanoparticles.

Following the rehydrogenation under 6 MPa hydrogen pressure at 350 °C after the first complete dehydrogenation, the second dehydrogenation of the sample is carried out. Fig. 9 exhibits the first dehydrogenation and the second dehydrogenation curves of the ball-milled MgH_2 doped with 7 mol% nanosized CoFe_2O_4 and the same amount of the ternary combination (Co_3Fe_7 , MgO and Co). There are obvious three phenomena: (1) The initial dehydrogenation temperature of the ball-milled MgH_2 doped with Co_3Fe_7 , MgO and Co is at about 260 °C, much lower than that of the as-milled MgH_2 , which starts to release hydrogen at around 360 °C, indicating that the combination of Co_3Fe_7 , MgO and Co shows great catalytic effect to advance MgH_2 hydrogen storage performance. (2) The ball-milled MgH_2 doped with Co_3Fe_7 , MgO and Co do not exhibit two different processes, and the onset desorption temperature is approximately 100 °C higher than that of the ball-milled MgH_2 doped with 7 mol% nanosized CoFe_2O_4 . (3) The initial temperatures of the second dehydrogenation of the ball-milled MgH_2 doped with the ternary combination (Co_3Fe_7 , MgO and Co) are almost the same as the first dehydrogenation, but decline by 60 °C, compared with that of the ball-milled MgH_2 doped with 7 mol% CoFe_2O_4 at the second dehydrogenation.

The reasons of the first phenomenon may be that the ternary combination (Co_3Fe_7 , MgO and Co) has a great catalytic effect on the hydrogen storage of MgH_2 . Transition metals catalysts play an important role in hydrogen storage properties of MgH_2 , and the most suitable transition metals catalysts require 6–9 electrons

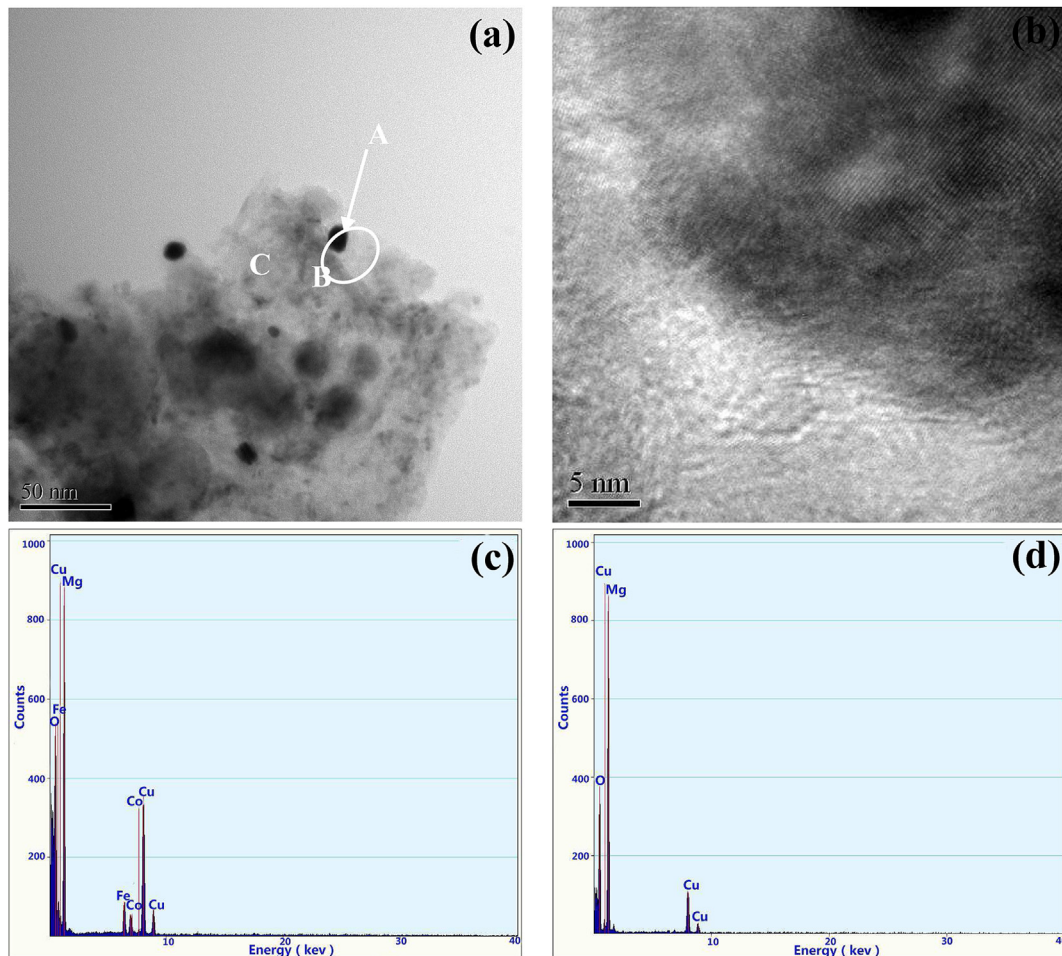


Fig. 12. (a) TEM morphology and (b) HRTEM boundaries micrographs of the black and bright regions, EDX: (c) black region, (d) bright region results of the ball-milled MgH_2 doped with the same amount of the ternary combination (Co_3Fe_7 , MgO and Co).

occupying the 3d orbit, such as Fe, Co, Ni. These transition metals easily absorb hydrogen atoms to fill the 3d orbits and make MgH_2 dynamically unstable [35]. Bobet et al. [36] also reported that the hydrogen storage properties of Mg were significantly improved after doping with 10 wt% Co, Ni or Fe by mechanical alloying in H_2 (reactive mechanical grinding) for 2 h. Meanwhile, Zhao et al. [37] also reported that the CoFe/MgO catalyst has more advantages accelerating the process of CO hydrogenation. Therefore, the mixture of Co_3Fe_7 , MgO and Co may have the same catalytic effect on the MgH_2 dehydrogenation.

The second phenomenon suggests that CoFe_2O_4 has better catalytic effect than the ternary combination (Co_3Fe_7 , MgO and Co) on the hydrogen storage of MgH_2 . CoFe_2O_4 has strong oxidative activity, while MgH_2 has strong reduction. Thus, MgH_2 can react with CoFe_2O_4 at a relatively low temperature. A similar phenomenon also appears when some other oxide catalysts are added into the MgH_2 matrix. For example, Nb_2O_5 [13], Fe_2O_3 and Co_3O_4 [17] catalysts, which all have strong oxidative activity, exhibit better catalytic performance. However, the catalytic performance of Al_2O_3 [14] and SiO_2 [17], which have relatively weak oxidation, is poor for improving hydrogen storage properties of MgH_2 . This point becomes even more obvious when Fe_2O_3 and Fe_3O_4 are selected as catalysts, as the catalyst effect of Fe_2O_3 , which has stronger oxidative activity than Fe_3O_4 , is also greater than Fe_3O_4 [38]. Thus, it is reasonable to believe that the great catalytic performance of

CoFe_2O_4 is determined in large by its strong oxidative activity. However, in the next hydriding–dehydriding process, CoFe_2O_4 cannot be kept stable and will decompose into other substances. This characteristic limits the CoFe_2O_4 catalysts practical applications.

CoFe_2O_4 nanoparticles play a role only during the first time of the MgH_2 dehydrogenation. In the second dehydrogenation, Co_3Fe_7 , MgO and Co are also the main phases that affect hydrogen storage properties of MgH_2 doped with CoFe_2O_4 , so the third phenomenon indicates that different methods of adding the catalysts have different effects on the MgH_2 hydriding–dehydriding processes. The morphology and microstructure of the mixed samples prepared by different doping methods were examined by transmission electron microscopy and the elemental composition of the tested sample was obtained by the energy dispersive X-ray spectroscopy. Figs. 10(a)–13(a) exhibit the distribution of the catalyst in the MgH_2 matrix. For the black region, Mg, O, Fe, Co and Cu elements are observed (shown in Figs. 10(c)–13(c)), and for the bright region, Mg, Cu and O elements are detected (shown in Figs. 10(d)–13(d)). Cu element comes from the 3 mm Cu grid, which is used as a carrier, and oxygen element in the bright region may be due to the sample contamination during preparation. These results indicate that the large bright particle is MgH_2 , and the black particle is the catalyst. According to the previous analysis, the black regions in Fig. 10(c) correspond to CoFe_2O_4 (Mg element is originated from the matrix).

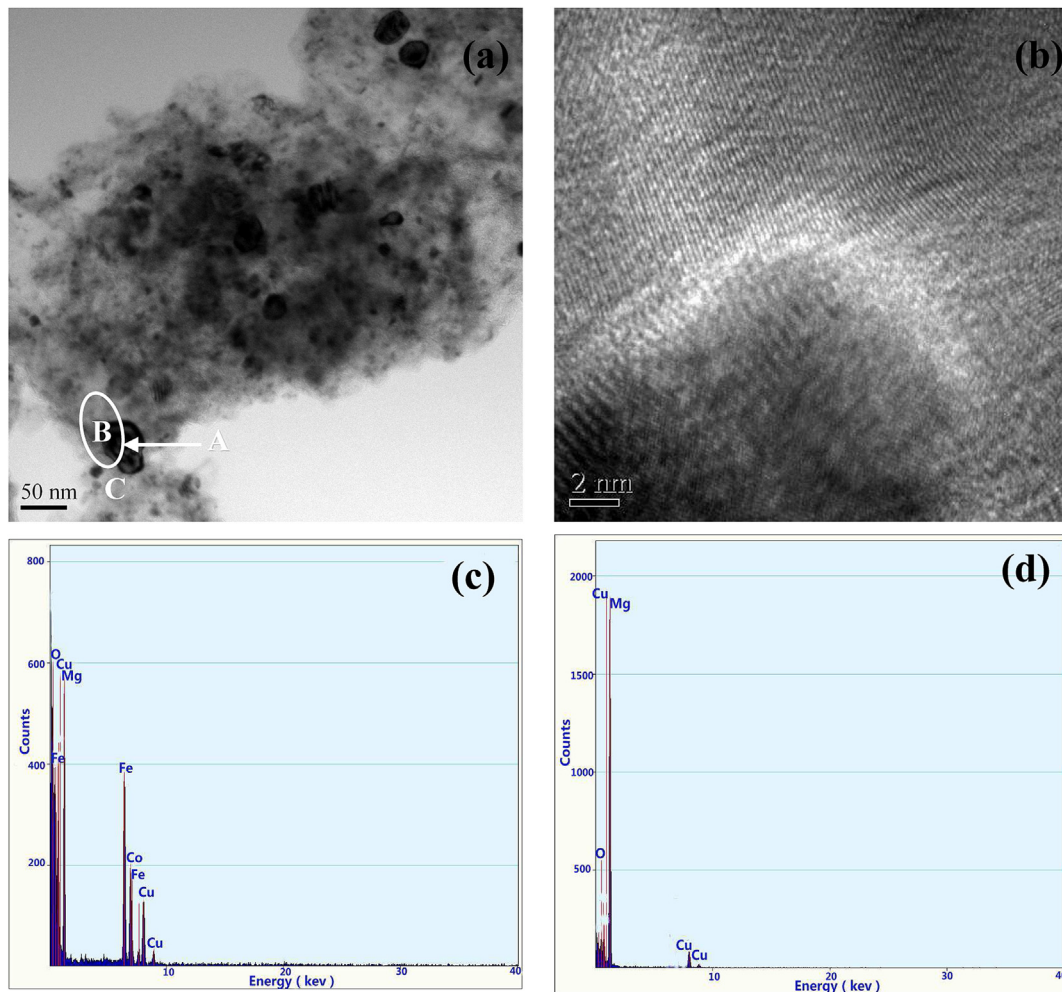


Fig. 13. (a) TEM morphology and (b) HRTEM boundaries micrographs of the black and bright regions, EDX (c) black region, (d) bright region results of the ball-milled MgH_2 doped with the same amount of the ternary combination (Co_3Fe_7 , MgO and Co) after the second dehydrogenation.

What's depicted in Figs. 11(c)–13(c) should be the ternary combination (Co_3Fe_7 , MgO and Co).

From Figs. 10 and 13, one can find that when the CoFe_2O_4 , or the ternary combination (Co_3Fe_7 , MgO and Co) is added in the MgH_2 matrix by the ball milling, they are uniformly distributed among the MgH_2 particles. To further reveal the combination mode of the catalysts with MgH_2 , HRTEM is performed and the results are shown in Figs. 10(b) and 13(b). It is clearly seen that the CoFe_2O_4 or the ternary combination (Co_3Fe_7 , MgO and Co) is inlaid into the MgH_2 matrix, and the boundaries appear as large number of defects, which will be the paths for hydrogen diffusion. Meanwhile, these defects provide the place for nucleation during the hydriding–dehydriding processes.

Comparing Figs. 10(b) and 11(b), the border regions of the ball-milled MgH_2 doped with 7 mol% nanosized CoFe_2O_4 fuse toward integration, and the defect density is significantly reduced after the second dehydrogenation. Perhaps the reason is that the atoms pad into the boundaries and the defects by diffusion during the chemical reaction between MgH_2 and CoFe_2O_4 . However, there is no change of the border regions and the defect density of the ball-milled MgH_2 doped with the ternary combination (Co_3Fe_7 , MgO and Co) after the two dehydrogenation cycles, shown in Figs. 12(b) and 13(b), explaining that the initial temperatures of the first dehydrogenation and the second dehydrogenation of the ball-milled MgH_2 doped with the ternary combination (Co_3Fe_7 , MgO and Co) are almost the same, but decline by 60 °C, compared with the ball-milled MgH_2 doped with 7 mol% CoFe_2O_4 at the second dehydrogenation.

From the above analyses, the CoFe_2O_4 role during the whole dehydrogenation process of MgH_2 can be demonstrated. CoFe_2O_4 reacts with MgH_2 matrix during the dehydrogenation process to form the ternary combination (Co_3Fe_7 , MgO and Co), and the newly formed ternary combination also acts as a catalyst to facilitate the MgH_2 decomposition.

4. Conclusions

The hydrogen storage properties of MgH_2 are dramatically enhanced by doping CoFe_2O_4 nanoparticles. The nonisothermal desorption results show that the onset desorption temperature of $\text{MgH}_2 + 7$ mol% CoFe_2O_4 is 160 °C, 200 °C lower than the as-milled MgH_2 . DTA curves reveal that MgH_2 can react with CoFe_2O_4 at a relatively low temperature, manifesting that CoFe_2O_4 has high catalytic effect on the hydrogen storage of MgH_2 , based on its strong oxidative activity. XRD patterns show that the final reaction products of MgH_2 and CoFe_2O_4 are the ternary combinations (Co_3Fe_7 , MgO and Co) with high chemical stability, indicating that CoFe_2O_4 nanoparticles only play a role during the first MgH_2 dehydrogenation. In the next hydriding–dehydriding cycles, Co_3Fe_7 , MgO and Co are the main phases that affect hydrogen storage properties of MgH_2 . The initial dehydrogenation temperature of the ball-milled MgH_2 doped with Co_3Fe_7 , MgO and Co is about 260 °C, much lower than the as-milled MgH_2 , which starts to release hydrogen at around 360 °C, manifesting that the combination of Co_3Fe_7 , MgO and Co significantly advances the MgH_2 hydrogen storage performance. The initial temperature of the second dehydrogenation of the ball-milled MgH_2 doped with the ternary combination (Co_3Fe_7 , MgO and Co) is almost the same the first dehydrogenation, but declined by 60 °C compared with the ball-milled MgH_2 doped with 7 mol% CoFe_2O_4 at the second dehydrogenation. The reasons are fusing of the border regions of the ball-milled MgH_2 doped with 7 mol% nanosized CoFe_2O_4 and the defect density significant reduction because of the atoms padding into the boundaries and the defects by diffusion during the

chemical reaction between MgH_2 and CoFe_2O_4 . However, there is no change of the border regions and the defect density of the ball-milled MgH_2 doped with the ternary combination (Co_3Fe_7 , MgO and Co) after the two dehydrogenation cycles.

Acknowledgments

The authors acknowledge the financial support from the National High-Tech R&D Program (863 Program) of China (2011AA03A408). Fuqiang Zhai thanks the China Scholarship Council (CSC) for providing the scholarship.

References

- [1] I.P. Jain, Int. J. Hydrogen Energy 34 (2009) 7368–7378.
- [2] J. Lu, Y.J. Choi, Z.Z. Fang, H.Y. Sohn, E. Rönnebro, J. Am. Chem. Soc. 131 (2009) 15843–15852.
- [3] H. Liu, X. Wang, Y. Liu, Z. Dong, G. Cao, S. Li, M. Yan, J. Mater. Chem. A 1 (2013) 12527.
- [4] J. Cui, H. Wang, J. Liu, L. Ouyang, Q. Zhang, D. Sun, X. Yao, M. Zhu, J. Mater. Chem. A 1 (2013) 5603.
- [5] I.P. Jain, C. Lal, A. Jain, Int. J. Hydrogen Energy 35 (2010) 5133–5144.
- [6] J. Mao, Z. Guo, X. Yu, H. Liu, Z. Wu, J. Ni, Int. J. Hydrogen Energy 35 (2010) 4569–4575.
- [7] M.Y. Song, Y.J. Kwak, H.R. Park, D.R. Mumm, Mater. Res. Bull. 46 (2011) 1887–1891.
- [8] C.X. Shang, M. Bououdina, Y. Song, Z.X. Guo, Int. J. Hydrogen Energy 29 (2004) 73–80.
- [9] M. Polanski, J. Bystrzycki, R.A. Varin, T. Plocinski, M. Pisarek, J. Alloys Compd. 509 (2011) 2386–2391.
- [10] C. Zhou, Z.Z. Fang, J. Lu, X. Zhang, J. Am. Chem. Soc. 135 (2013) 10982–10985.
- [11] J. Zhang, W. Zaïdi, V. Paul-Boncour, K. Provost, A. Michalowicz, F. Cuevas, M. Latroche, S. Belin, J. Bonnet, L. Aymard, J. Mater. Chem. A 1 (2013) 4706.
- [12] N. Hanada, T. Ichikawa, S. Isobe, T. Nakagawa, K. Tokoyoda, T. Honma, H. Fujii, Y. Kojima, J. Phys. Chem. C 113 (2009) 13450–13455.
- [13] T.K. Nielsen, T.R. Jensen, Int. J. Hydrogen Energy 37 (2012) 13409–13416.
- [14] W. Oelerich, T. Klassen, R. Bormann, J. Alloys Compd. 315 (2001) 237–242.
- [15] S. Milošević, Ž. Rašković-Lovre, S. Kurko, R. Vujasin, N. Cvjetičanin, L. Matović, J. Grbović Novaković, Ceram. Int. 39 (2013) 51–56.
- [16] A. Patah, A. Takasaki, J.S. Szmyd, Int. J. Hydrogen Energy 34 (2009) 3032–3037.
- [17] H. Yuan, X. Zhang, Z. Li, J. Ye, X. Guo, S. Wang, X. Liu, L. Jiang, Int. J. Hydrogen Energy 37 (2012) 3292–3297.
- [18] K. Wang, X. Kang, Q. Kang, Y. Zhong, C. Hu, P. Wang, J. Mater. Chem. A 2 (2014) 2146.
- [19] L.P. Ma, X.D. Kang, H.B. Dai, Y. Liang, Z.Z. Fang, P.J. Wang, P. Wang, H.M. Cheng, (2009).
- [20] S. Rather, R. Zacharia, C.S. So, S.W. Hwang, A.R. Kim, K.S. Nahm, J. Alloys Compd. 471 (2009) L16–L22.
- [21] M. Park, J. Shim, Y. Lee, Y.H. Im, Y.W. Cho, J. Alloys Compd. 575 (2013) 393–398.
- [22] M.O.T. Da Conceição, M.C. Brum, C.S. Guimarães, D.S. Dos Santos, J. Alloys Compd. 536 (2012) S255–S258.
- [23] N. Mahmoudi, A. Kafilou, A. Simchi, J. Power Sources 196 (2011) 4604–4608.
- [24] K. Takahashi, S. Isobe, S. Ohnuki, J. Alloys Compd. 580 (2013) S25–S28.
- [25] Z. Li, P. Li, Q. Wan, F. Zhai, Z. Liu, K. Zhao, L. Wang, S. Lü, L. Zou, X. Qu, A.A. Volinsky, J. Phys. Chem. C 117 (2013) 18343–18352.
- [26] T. Mandzhukova, M. Khrussanova, E. Grigorova, P. Stefanov, M. Khristov, P. Peshev, J. Alloys Compd. 457 (2008) 472–476.
- [27] P. Li, Z. Li, F. Zhai, Q. Wan, X. Li, X. Qu, A.A. Volinsky, J. Phys. Chem. C 117 (2013) 25917–25925.
- [28] Z. Li, F. Zhai, Q. Wan, Z. Liu, J. Shan, P. Li, A. Volinsky, X. Qu, RSC Adv. 36 (2014) 18989–18997.
- [29] P. Li, Q. Wan, Z. Li, F. Zhai, Y. Li, L. Cui, X. Qu, A.A. Volinsky, J. Power Sources 239 (2013) 201–206.
- [30] E.N. Koukaras, A.D. Zdetsis, M.M. Sigalas, J. Am. Chem. Soc. 134 (2012) 15914–15922.
- [31] R. Floriano, D.R. Leiva, S. Deledda, B.C. Hauback, W.J. Botta, Int. J. Hydrogen Energy 38 (2013) 16193–16198.
- [32] M. Paskevicius, D.A. Sheppard, C.E. Buckley, J. Am. Chem. Soc. 132 (2010) 5077–5083.
- [33] L. Xi, Z. Wang, Y. Zuo, X. Shi, Nanotechnology 22 (2011) 45707.
- [34] N. Hanada, T. Ichikawa, H. Fujii, J. Phys. Chem. B 109 (2005) 7188–7194.
- [35] J. Harris, S. Andersson, C. Holmberg, P. Nordlander, Phys. Scr. 1986 (1986) 155.
- [36] J. Bobet, E. Akiba, Y. Nakamura, B. Darriet, Int. J. Hydrogen Energy 25 (2000) 987–996.
- [37] J. Zhai, J. Beijing Univ. Chem. Technol. (2012).
- [38] Z.G. Huang, Z.P. Guo, A. Calka, D. Wexler, C. Lukey, H.K. Liu, J. Alloys Compd. 422 (2006) 299–304.